Catalysis Today 149 (2010) 309–315

Contents lists available at ScienceDirect

Catalysis Today

journal homepage: www.elsevier.com/locate/cattod

# Mn/Mg/Al-spinels as catalysts for $SO_x$ abatement Influence of $CeO_2$ incorporation and catalytic stability

Hugo B. Pereira [a], Carla M.S. Polato [b], José Luiz F. Monteiro [c], Cristiane A. Henriques [a,*]

[a] IQ/UERJ, Rua São Francisco Xavier, 524, CEP 20550-900, Rio de Janeiro, Brazil
[b] INPI, Instituto Nacional de Propriedade Industrial, Rio de Janeiro, Brazil
[c] NUCAT–COPPE/UFRJ, PO Box 68502, CEP 21945-970, Rio de Janeiro, Brazil

ARTICLE INFO

*Article history:*
Available online 30 July 2009

*Keywords:*
$SO_x$ abatement
Mn/Mg/Al spinels
Hydrotalcites
Sulfur-transfer additives
$DeSO_x$
Mn-containing catalysts
$CeO_2$

ABSTRACT

Mg,Mn,Al-oxides with spinel structure, Al/($M^{2+}$ + Al) molar ratio of 0.25 and 0.50 and an Mn/Mg molar ratio of 0.30 have been evaluated as catalysts for $SO_x$ removal under conditions similar to those found in FCC units. The best performance was that of the sample with the higher aluminium content. The incorporation of $CeO_2$ in this sample favored $SO_x$ uptake for short reaction times as well as the reduction of the sulfated catalysts. When the regeneration was started at 530 °C, only $H_2S$ was observed as reaction product, but when this step started at 650 °C, the release of $SO_2$ preceded that of $H_2S$, regardless of the chemical composition of the sample. As to the additive performance for successive reaction–regeneration cycles, the incorporation of $CeO_2$ produced a less efficient catalyst with regard to the removal of the $SO_2$ along the process, but with a higher regeneration efficiency and a lower formation of $SO_2$ as regeneration product.



## 1. Introduction

The growing concern about the environment has resulted in stringent legislations for the control of $SO_x$ emissions from industrial and power plants. As to the oil refineries, FCC units are the major individual source of $SO_x$ emissions. Although the relative contribution of the refineries, in comparison with the total amount of $SO_x$ emitted by the different sources, is relatively small (6–10%), it can become very significant in areas already saturated or in industrial complexes [1]. Thus, these emissions of pollutant gases ($SO_x$, $NO_x$, CO) are under regulation of specific legislation in several countries.

The worldwide trend of processing heavier petroleum fractions also contribute to the increase of $SO_x$ and $NO_x$ emissions in the refineries since they are richer in sulfur and nitrogen compounds. This problem can be controlled by lowering the concentration of nitrogen and sulfur compounds by hydrotreating the feed. However, this alternative is very costly and not always technologically possible. An economically viable option for the reduction of the emissions of $SO_x$ is the addition of sulfur-transfer additives to the FCC catalyst. These additives adsorb $SO_x$ and so transfer sulfur back into the riser where it is released as $H_2S$, which is removed in the usual way (Claus process). This technique is very practical since the use of additives requires almost no capital investment, except for the cost of an additive loading system and the availability of a Claus plant. Three steps determine the performance of a $SO_x$ transfer catalyst: (1) oxidation of $SO_2$ to $SO_3$ under the FCC regenerator conditions, typically at 700–730 °C, (2) trapping of $SO_3$ on the catalyst in the form of sulfates, and (3) reduction of sulfates to release sulfur as $H_2S$ in the FCC riser, typically at 520–530 °C [2–6].

As to the catalyst formulation, mixed oxides and/or spinels prepared from hydrotalcite-like compounds (HTLCs or LDHs) have been proved to be good sulfur-transfer catalysts [2–11], since they offer a large capacity of adsorption of $SO_3$, forming moderately stable metal sulfates under the conditions of the regenerator that can be decomposed in the reductive atmosphere of the cracking zone. The presence of $SO_2$ oxidation promoters as co-catalysts is also necessary since the $SO_3$ content in the regenerator is relatively low (about 10% $SO_3$ and 90% $SO_2$).

Literature reports the incorporation of different metallic oxides such as those of Ce, Cu, Co, V, Cr, and Fe to hydrotalcite-like compounds (HTLC) either by impregnation or co-precipitation as the best way to generate the mixed oxides/spinels solid solutions with both basic and redox properties needed for good performance in the De–$SO_x$ process [3–5,7,9–15]. The incorporation of manganese oxides is also an interesting option, since it is well known that they are efficient catalysts for processes that involve redox reactions, due to different oxidation states (+2, +3, +4 and +7) that the element can assume [16–19]. Particularly to the $SO_x$

* Corresponding author. Fax: +55 21 23340159.
*E-mail address:* cah@uerj.br (C.A. Henriques).

0920-5861/$ – see front matter © 2009 Elsevier B.V. All rights reserved.
doi:10.1016/j.cattod.2009.06.006

removal processes, manganese oxide-based catalysts have been investigated as traps for $SO_x$ uptake from the exhaustion gases of both diesel and gasoline engines in order to increase the useful life of the automotive catalysts [20,21]. Furthermore, promising results of the use of Mg,Mn,Al-oxides with spinel structure as additive for $SO_x$ removal in FCC units were recently reported by Polato et al. [22,23]. However, additional investigations are still needed for a more complete comprehension of their performance in the real process.

Several properties must be taken into account so that a given material can be incorporated to the FCC catalyst as additive for $SO_x$ abatement. Thus, besides the efficiency for $SO_2$ capture as sulfate and its release as $H_2S$, the other aspects that should be investigated are its performance after incorporation to the equilibrium catalyst, including the resistance to hydrothermal deactivation associated to the steaming at the high temperatures of the regenerator, its stability toward successive cycles of reaction–regeneration, and the effect of the presence of other pollutant, such as $NO_x$ and CO, also present in the regenerator due to the coke burning, on the $SO_x$ removal efficiency.

Aiming at to continue our studies on Mn-containing sulfur-transfer catalysts, in this work Mn,Mg,Al-oxides with spinel structure, different $Al/(M^{2+} + Al)$ molar ratios (0.25 or 0.50) and Mn/Mg of 0.30 were examined as potential catalysts for $SO_x$ removal under conditions similar to those found in the FCC units. The effect of the incorporation of $CeO_2$ as well as the stability of the catalysts along successive cycles of reaction and regeneration has also been evaluated.

## 2. Experimental

### 2.1. Catalyst synthesis

Hydrotalcite-like samples (HTLCs) were prepared by co-precipitation, at room temperature. Solution A, containing the metallic cations dissolved in distilled water ((Al + Mg + Mn) = 1.5 - mol/L; $Al/(Al + M^{2+})$ = 0.25 or 0.50 and Mn/Mg = 0.30) was slowly dropped to solution B, prepared by dissolving $Na_2CO_3$ and NaOH in distilled water in order to obtain a $[CO_3^{2-}]$ equal to 1.0 mol/L and a pH equal to 13 during the aging of the gel. The gel formed was aged under constant pH (13) for 18 h at 333 K. The solid obtained was filtered, washed with distilled water (363 K) until pH 7 and dried at 353 K overnight. The synthesized samples were named MnHTX where X is the $Al/(Al + M^{2+})$ molar ratio.

The mixed oxides and/or spinels were obtained by calcining HTLC precursors under dry air from room temperature to 1023 K, using a heating rate of 10 K/min. They were named MnMOX, where MO means mixed oxide and X is defined as above.

Part of the MnMO50 sample was wet impregnated with a 25 mol/L $Ce(NO_3)_3{\cdot}6H_2O$ solution in a rotavapor at 333 K in order to incorporate 17 wt.% of $CeO_2$ in the catalyst. The material was dried overnight at 393 K and then calcined at 1023 K for 2 h. This sample was named $CeO_2$/MnMO50. The solids were crushed and sieved to the range 63–105 μm (−150 + 250 mesh Tyler).

### 2.2. Physico-chemical characterization

The chemical composition of the synthesized samples was determined by X-ray fluorescence using a Rigaku Rix 3100 spectrometer. X-ray powder diffraction patterns were recorded in Rigaku X-Ray Diffractometer equipped with a graphite monochromator using Cu Kα, 40 kV, and 40 mA, in the range $2\theta$ from 10° to 80°. The textural characteristics such as specific surface area (BET), external area (*t*-plot), and pore volume (BJH) were determined by $N_2$ adsorption–desorption at 77 K in a Micromeritics ASAP 2000. The samples were previously outgassed at 473 K overnight.

### 2.3. Catalytic tests

The catalytic tests were conducted in a fixed bed quartz microreactor using 30 mg of catalyst. Two sets of experiments were carried out. In the first, for the $SO_2$ oxidative adsorption step, a stream of 175 mL/min with 1630 ppm of $SO_2$, 1.6% (v/v) of $O_2$, and He balance was passed over the catalyst at 720 °C during 10 min. For catalyst regeneration, the system was flushed with He and the sample was cooled down to 530 °C. Then, He was shut off and the catalyst was reduced in a stream of 130 mL/min of $H_2$(30%)/He(70%) for 30 min, at 530 °C. After that, the temperature was ramped to 800 °C at 5.4 °C/min, under the same atmosphere (TPR stage).

In the second set of experiments, the initial temperature of the regeneration step has been increased to 650 °C (temperature of the catalyst when it enters in the base of the riser coming from the regenerator) and the time on stream associated to the isothermal stage has been reduced to 5 min (minimum time for the acquisition of sufficient points to establish the reduction profile for this stage). Thus, the sulfated catalysts were reduced under $H_2$(30%)/He(70%) stream (130 mL/min) for 5 min, at 650 °C. After that, the temperature was increased to 800 °C at 5.4 °C/min, under the same atmosphere. For the $SO_2$ oxidative adsorption step, the time on stream was increased to 35 min, the other experimental conditions being kept constant (720 °C; 1630 ppm $SO_2$, 1.6 vol.% $O_2$, and He balance). The times on stream of 35 min (oxidative adsorption) and 5 min (regeneration) were selected in order to use a regenerator/riser average residence time ratio representative of that usually found in the FCC units (regenerator/*riser* ≈ 7:1) [12,24].

The stability of the studied catalysts was evaluated along 21 successive cycles of reaction–regeneration. The experimental conditions were those described for the second set of experiments, without the TPR stage in the regeneration step. At the end of each regeneration step, the reactor was purged with He, the temperature was raised from 650 to 720 °C and a new cycle began.

The reaction products were analyzed by on line gas chromatography using a VARIAN Micro GC, model CP-4900, equipped with a thermal conductivity detector and a PPQ column (10 m).

## 3. Results and discussion

### 3.1. Physico-chemical characterization

The X-ray diffractograms of the as-synthesized samples are shown in Fig. 1. For sample MnHT25, small diffraction peaks corresponding to a $Mn_3O_4$–hausmanite-type phase [25] were observed along with those of the hydrotalcite phase, indicating that part of the $Mn^{2+}$ cations was transformed into $Mn^{3+}$ during the synthesis, as previously suggested by Velu et al. [16], since, according to the redox potentials, the oxidation of $Mn^{2+}$ to $Mn^{3+}$ is highly favorable in a basic medium typical of the synthesis gel. For sample MnHT50, besides the hydrotalcite peaks, diffraction lines corresponding to a bayerite (aluminium hydroxide, $Al(OH)_3$) phase [25] were also observed. The segregation of this phase is commonly observed for HTLCs with $Al/(Al + M^{2+})$ molar ratios greater than 0.33 and can be associated to the increase in the number of neighboring $Al^{3+}$ ions in the hydroxide layers, so exceeding the repulsion among the positive charges that are responsible for keeping distant the $Al^{3+}$ ions [26]. Differently to that observed for MnHT25 (sample with higher manganese content), manganese species ($Mn^{2+}$ and $Mn^{3+}$) were completely incorporated into the lamellar structure of sample MnHT50, confirming the suggestion

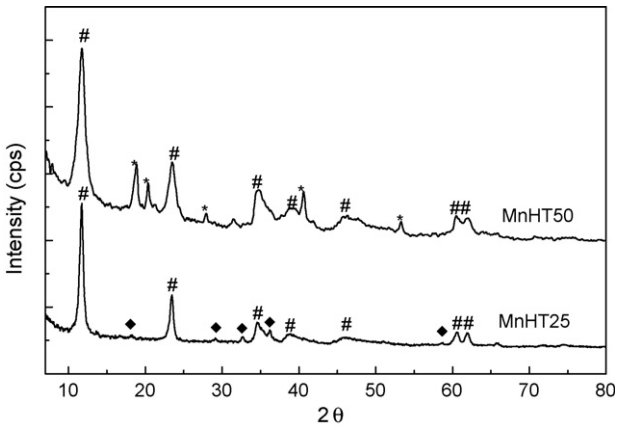


**Fig. 1.** X-ray diffractograms of the as-synthesized HTLCs. (#) Hydrotalcite; (◆) $Mn_3O_4$–hausmanite; (*) $Al(OH)_3$–bayerite.

of Velu et al. [16] that there is a limit amount of (Al + Mg) ions that can be isomorphously substituted by Mn species in the brucite-like layer of the HTLC.

As shown in Fig. 2, upon calcination at 750 °C, the lamellar structure of HTLCs collapsed and the X-ray diffractogram of MnMO50 shows the formation of a poorly crystallized Mg,Mn,Al-oxides with a cubic spinel-type structure [25] and a lattice parameter ($a$ = 8.256 Å) intermediate between those of $MgAl_2O_4$ ($a$ = 8.083 Å) and $MnAl_2O_4$ ($a$ = 8.371 Å) spinels [25]. Due to the broadness of the XRD peaks, their exact assignment to a well-defined phase was not possible. A similar behavior was observed for sample MnMO25, whose X-ray diffractogram indicates the disappearance of the LDH and of the $Mn_3O_4$–hausmanite phases and the formation of the Mg,Mn,Al-oxide phase with an spinel structure (Fig. 2). However, for this sample, the diffraction peak at 18.7° was sharper and well-defined suggesting the segregation of a Mg,Mn-oxide with cubic structure ($a$ = 8.381 Å) [25].

For the sample impregnated with cerium and re-calcined at 750 °C ($CeO_2$/MnMO50), Fig. 2 also shown that the original Mg,Mn,Al-oxide phase did not suffer any modification and diffraction peaks associated to the $CeO_2$ phase with a cerianite structure [25] were also observed.

Table 1 shows the main results of chemical analysis and textural characteristics of the studied catalysts. The chemical composition indicates that the metallic cations were incorporated at the expected levels as well as the $CeO_2$. All the studied catalysts were mesoporous solids. However, the introduction of $CeO_2$ on sample MnMO50 partially blocked its porous structure, influencing significantly the pore size distribution. As can be seen in Fig. 3, pores with diameter lower than 50 Å or greater than 200 Å were blocked and the bimodal porous distribution of sample MnMO50 disappeared. Thus, $CeO_2$/MnMO50 presented a unimodal pore size distribution in the range 50–250 Å.

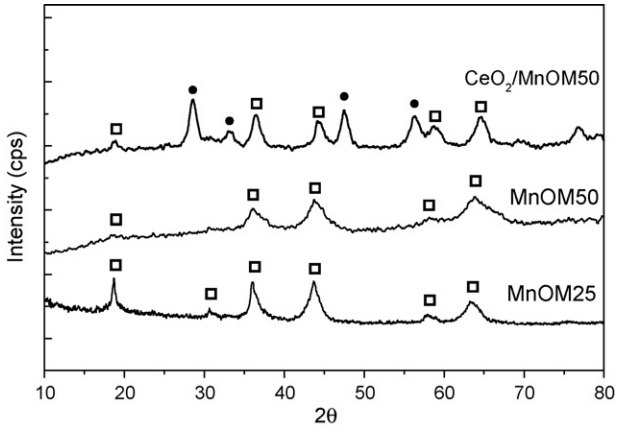


**Fig. 2.** X-ray diffractograms of the calcined samples. (□) Mn,Mg,Al-oxide spinel; (●) $CeO_2$–cerianite.

**Table 1**
Chemical composition and textural characteristics of the catalysts.

| Sample | Atomic ratio | | $CeO_2$ (wt.%) | $S_{BET}$ ($m^2$/g) | $V_{meso}$ ($cm^3$/g) |
|---|---|---|---|---|---|
| | Al/(Al + Mg + Mn) | Mn/Mg | | | |
| MnMO25 | 0.23 | 0.26 | – | 113 | 0.569 |
| MnMO50 | 0.46 | 0.29 | – | 211 | 0.463 |
| $CeO_2$/MnMO50 | 0.46 | 0.29 | 17 | 129 | 0.336 |

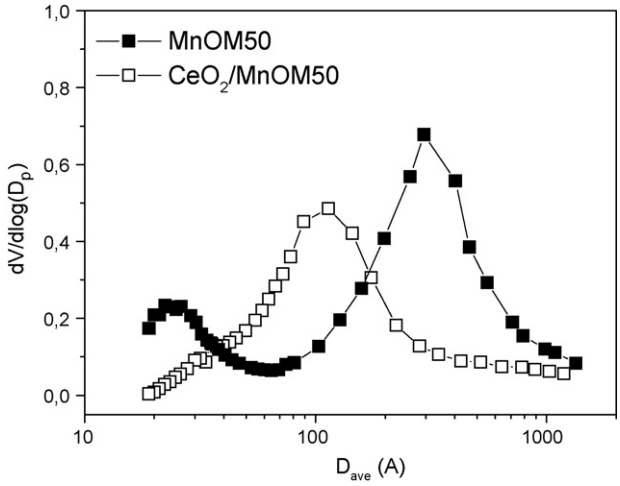


**Fig. 3.** Pore size distribution for samples MnMO50 and $CeO_2$/MnMO50.

### 3.2. Catalytic tests

#### 3.2.1. Influence of the chemical composition on catalysts performance

The performance of the studied catalysts in the $DeSO_x$ process was initially compared performing the oxidative adsorption at 720 °C, for 10 min, and the regeneration step at 530 °C for 30 min. Under these conditions, the reduction of the sulfated catalysts was not observed. So, the temperature was raised to 800 °C at 5.4 °C/min, under the same reductive stream (30 vol.% $H_2$/He). As to the influence of the Al/(Al + $M^{2+}$) molar ratio, Table 2 shows that sample MnOM50 presents not only a higher $SO_2$ pick-up capacity than sample MnMO25 but also a higher regeneration efficiency. Similar trends were reported by Polato et al. [9] studying $CeO_2$-containing Mg,Al-mixed oxides/spinels with different Al/(Al + $M^{2+}$) molar ratios (0.25, 0.50 and 0.75) and by Pereira et al. [27], investigating Cu/Mg/Al-mixed oxides.

**Table 2**
Catalytic performance of the additives. Oxidative adsorption: 720 °C, 10 min, 1630 ppm $SO_2$, 1.6% (v/v) $O_2$, and He balance; regeneration: 30% $H_2$/He, 30 min at 530 °C + TPR up to 800 °C.

| Step | | Sample | | |
|---|---|---|---|---|
| | | MnOM25 | MnOM50 | Ce/MnOM50 |
| Oxidative adsorption | $SO_2$ pick-up (μmol/g) | 2639 | 3273 | 3719 |
| Regeneration | $SO_2$ released (μmol/g) | 4 | – | – |
| | $H_2S$ released (μmol/g) | 705 | 1675 | 2389 |
| | Regeneration (%) | 27 | 51 | 64 |

The incorporation of $CeO_2$ on sample MnOM50 had a beneficial effect since it increased the $SO_2$ removal and the reduction of the sulfated catalyst. The role of ceria is derived from its basic/redox character. Ceria reducibility enhances the oxidation of $SO_2$ to $SO_3$ under FCC regeneration conditions by reacting with $SO_2$ to give substoichiometric cerium oxide, which is then reoxidized by oxygen [28].

$$xSO_2(g) + CeO_2(s) \leftrightarrow xSO_3(g) + CeO_{2-x}(s) \quad (1)$$

$$CeO_{2-x}(s) + 1/2xO_2(g) \leftrightarrow CeO_2(s) \quad (2)$$

In addition, it helps the desorption of sulfates as hydrogen sulfide under reductive conditions. According to Trovarelli et al. [28], the basic character of $CeO_2$ would favor the adsorption of $SO_2$/$SO_3$ with formation of sulfates, but this hypothesis was not confirmed in the present work.

Taking into account the $SO_x$ uptake capacity previously reported for Mg,Al-mixed oxides with Al/(Al + Mg) molar ratio equal to 0.25 and 0.50 (400 and 381 μmol $SO_2$/g, after 4 h TOS, respectively) [9]; the results shown in Table 2 confirm the suggestion that the presence of the additional component with redox properties is fundamental for the use of spinels/mixed oxides derived from hydrotalcites as additives for $SO_x$ removal [9,10].

Fig. 4 compares the profiles of $H_2S$ released during the TPR stage (beginning at 530 °C) for samples MnOM50 and $CeO_2$/MnOM50. Although the incorporation of $CeO_2$ had a positive effect on the efficiency of additive regeneration, it did not influence the range of temperatures for reduction (560–680 °C; maximum at 620 °C).

### 3.3. Catalysts deactivation

The experimental conditions explored in the oxidative adsorption step can be considered as truly representative of those practiced in the regenerator of FCC units (720 °C, 10 min). However, concerning the reduction step, the time on stream of 30 min is much higher than the residence time in the riser. Moreover, the analysis of the regeneration profiles indicated that the reduction of the sulfated additives occurs at temperatures higher than 530 °C. Thus, the study of the stability of the catalysts during successive cycles of reaction–regeneration was carried out under different experimental conditions. The temperature of the regeneration step was increased to 650 °C, trying to simulate the temperature of the catalyst when it enters in the base of the riser coming from the regenerator, and time on stream was reduced to 5 min. In order to keep the proportion of 1:7 between the residence times in the riser and in the regenerator [12,24], the time on stream of the oxidative adsorption step was increased to 35 min and the other conditions kept constant.

**Table 3**
Catalytic performance of the additives. Oxidative adsorption: 720 °C, 35 min, 1630 ppm $SO_2$, 1.6% (v/v) $O_2$, and He balance; regeneration: 30% $H_2$/He, 5 min at 650 °C + TPR up to 800 °C.

| Step | | Sample | |
|---|---|---|---|
| | | MnOM50 | Ce/MnOM50 |
| Oxidative adsorption | $SO_2$ uptake (μmol/g) | 7416 | 6747 |
| Regeneration | $SO_2$ released (μmol/g) | 848 | 319 |
| | $H_2S$ released (μmol/g) | 4894 | 5113 |
| | Regeneration (%) | 77 | 81 |

The performance of samples MnOM50 and $CeO_2$/MnOM50 was initially compared under these new experimental conditions for a unique cycle of reaction–regeneration (Table 3). It can be observed that after 35 min TOS, the cerium-containing sample captures a lower amount of $SO_2$ than sample MnMO50. The analysis of the profiles of $SO_2$ removed along the reaction (Fig. 5) suggests that, for short reaction times (TOS ≤ 10 min), a positive effect of the incorporation of $CeO_2$ on $SO_2$ capture can be observed, confirming our previous results (Table 2). However, for larger reaction times, the amount of $SO_2$ removed decreased, reflecting the stronger deactivation of the ceria-containing catalysts. As shown by Polato et al. [9], the pore blockage due the growth of sulfate species is the main cause of deactivation of the $SO_x$ transfer catalysts, since both BET specific area and mesoporous volume markedly decreases as the amount of $SO_2$ captured increases. Thus, it can be suggested that for lower TOS, the pore blockage is not significant and the beneficial effect of $CeO_2$ prevails. As the amount of captured sulfate increases, the pore blockage becomes gradually more important, particularly for the most active sample, and the access of $SO_2$ to the active sites is restrained causing a more important deactivation.

When the regeneration step started at 650 °C, $SO_2$ was formed as the initial product of the reduction of the sulfated species, differently to that observed for the regeneration starting at 530 °C, when it was not detected at all. After 2 min TOS, the formation of $SO_2$ ceased and only $H_2S$ was detected as reduction product even during the TPR stage (heating up to 800 °C) (Figs. 6 and 7). It should also be mentioned that no decomposition of the sulfate species was observed under inert atmosphere at 650 °C. Thus, the observed results are in accordance with the proposition of Kim and Juskelis [13], according to which the reduction of the sulfate species ($S^{6+}$ to $S^{2-}$) is a consecutive sequence of reaction having $S^{4+}$ species as intermediates.

XRD analysis of samples MnMO50 and $CeO_2$/MnMO50 before and after the oxidative adsorption step (Figs. 8 and 9, respectively)

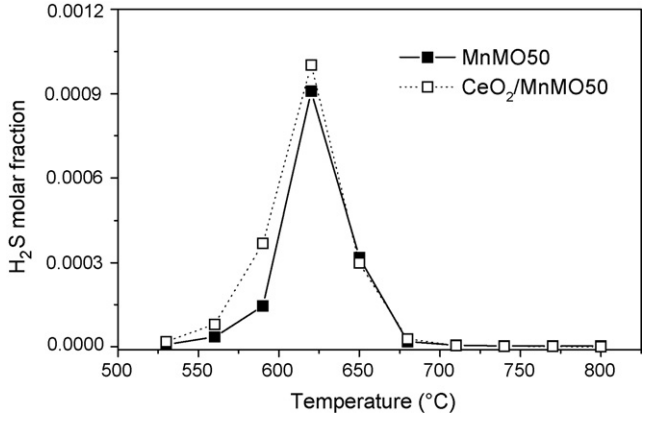


**Fig. 4.** Reduction profiles for sulfated MnOM50 and $CeO_2$/MnOM50 samples during the TPR stage (30% $H_2$/He; temperature ramped from 530 to 800 °C).

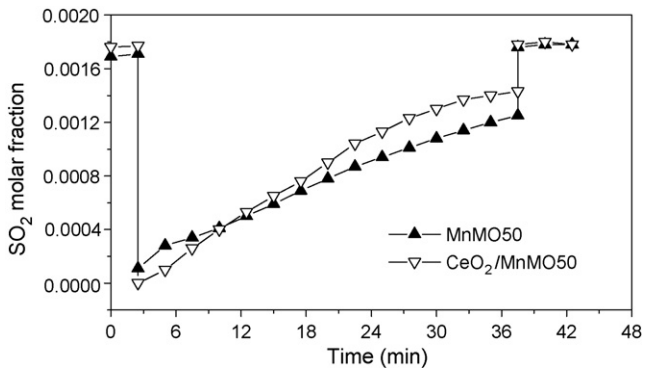


**Fig. 5.** $SO_2$ adsorption profiles for samples MnOM50 and $CeO_2$/MnOM50 (720 °C; 35 min; 1630 ppm $SO_2$, 1.6% (v/v) $O_2$ and He balance).

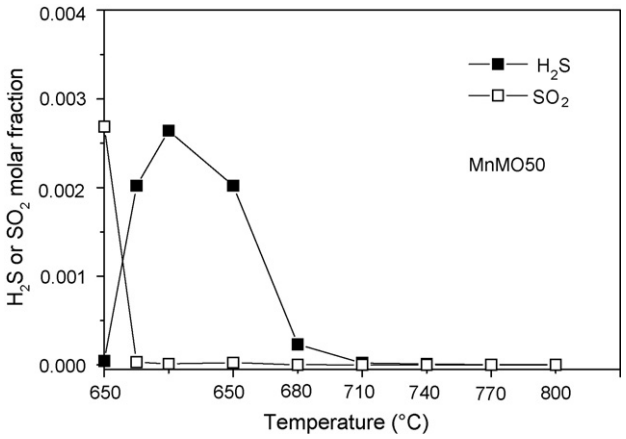


**Fig. 6.** Reduction profile for sulfated MnOM50 sample (30% $H_2$/He at 650 °C for 5 min; then, temperature was ramped to 800 °C).

indicated that the Mg,Mn,Al-oxide phase with spinel structure disappeared upon sulfation with the formation of $MgSO_4$ [25] and the segregation of a new phase corresponding to a Mg,Al-spinel ($MgAl_2O_4$) [25]. $CeO_2$–cerianite phase did not show any significant variation. This confirms that magnesium oxide is the active species for $SO_2$ oxidative adsorption, although the formation of a low crystallinity $MnSO_4$-phase from manganese(III) oxide could not be discharged according to the thermodynamic study carried out by Pereira et al. [29].

After the reduction of the sulfated additives, the $MgSO_4$-phase disappears forming a Mg(Mn,Al)O–periclase phase. The formation of an MnS–alabandite phase [25] is also observed. This fact can be considered as a strong evidence of the formation of $MnSO_4$, probably as small particles, not detected by XRD, since this compound can be reduced by hydrogen forming MnS.

$$2MnSO_4(s) + 5H_2(g) \rightarrow MnO(s) + MnS(s) + SO_2(g) + 5H_2O(g) \quad (3)$$

The presence of the $MgAl_2O_4$-spinel phase, whose peaks become sharper and well-defined, along with the Mg(Mn,Al)O–periclase phase, indicate the occurrence of permanent structural changes that prevent the recovery of the original Mg,Mn,Al-oxide with spinel structure.

At 650 °C, reaction (3) would occur at a higher rate than the reduction of $MgSO_4$

$$MgSO_4(s) + 4H_2(g) \rightarrow MgO(s) + 3H_2O(g) + H_2S(g) \quad (4)$$

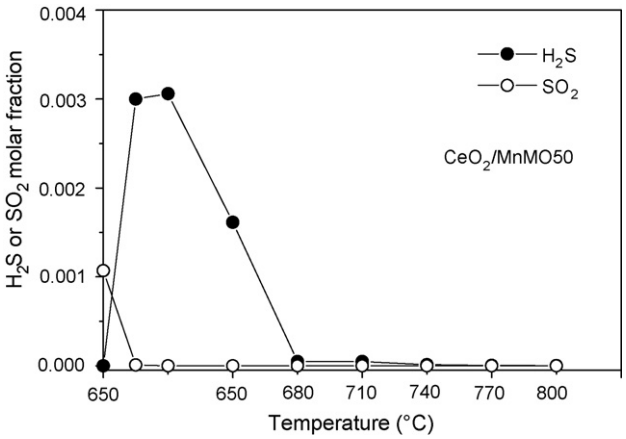


**Fig. 7.** Reduction profile for sulfated $CeO_2$/MnOM50 sample (30% $H_2$/He at 650 °C for 5 min; then, temperature was ramped to 800 °C).

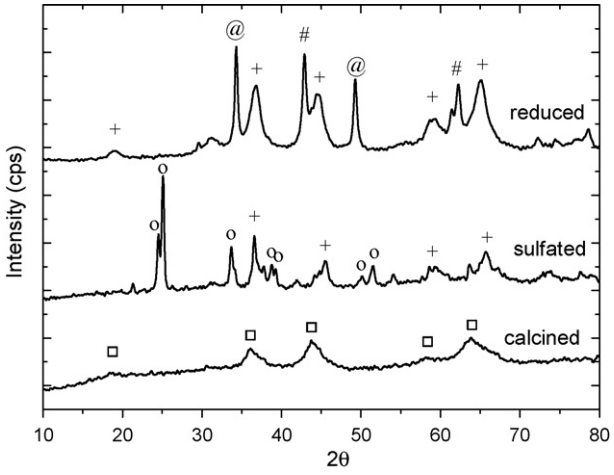


**Fig. 8.** X-ray diffractograms for sample MnOM50 before and after sulfation and after regeneration. (o) $MgSO_4$; (#) Mg(Mn,Al)O-periclase; (□) Mn,Mg,Al-oxide spinel structure; (+) $MgAl_2O_4$-spinel; (@) MnS–alabandite.

so justifying the detection of $SO_2$ as the initial product of the reduction of the sulfated catalysts. On the other hand, this hypothesis did not explain why the formation of $SO_2$ was not observed when the temperature reached 650 °C on the TPR stage starting at 530 °C (item 3.1). This fact can be tentatively explained considering that for short TOS (10 min) the amount of $MnSO_4$ formed in the oxidative adsorption step is lower and, consequently, $SO_2$ is released in small amounts, below the limit of detection of the analysis. The increase in the TOS to 35 min, not only increased the amount of captured sulfate but also the formation of $MnSO_4$. As a consequence, $SO_2$ was formed as reduction product in detectable amounts.

The beneficial effect of the incorporation of the $CeO_2$ on the regeneration of the sulfated catalysts was confirmed by both the increase in the catalyst regeneration and the significant reduction of the amount of $SO_2$ released.

The stability of the additives MnMO50 and $CeO_2$/MnMO50 was evaluated along 21 successive cycles of reaction–reduction. Fig. 10 shows the amount of $SO_2$ removed in the oxidative adsorption step along the successive cycles. Although both samples deactivate along the process, this effect is more significant for sample $CeO_2$/MnMO50, particularly in first five cycles. After the 20th first cycle, sample MnMO50 lost about 35% of its initial $SO_2$ uptake capacity while for sample $CeO_2$/MnMO50 the loss was near 50%.

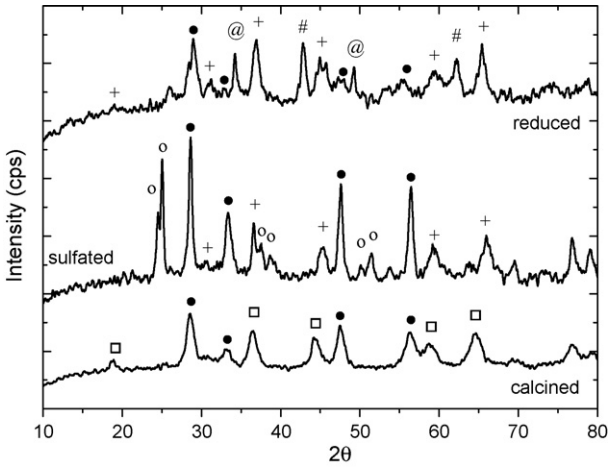


**Fig. 9.** X-ray diffractograms for sample $CeO_2$/MnOM50 before and after sulfation and after regeneration. (o) $MgSO_4$; (#) Mg(Mn,Al)O–periclase; (□) Mg,Mn,Al-oxide spinel structure; (+) $MgAl_2O_4$-spinel; (@) MnS–alabandite; (*) $CeO_2$–cerianite.

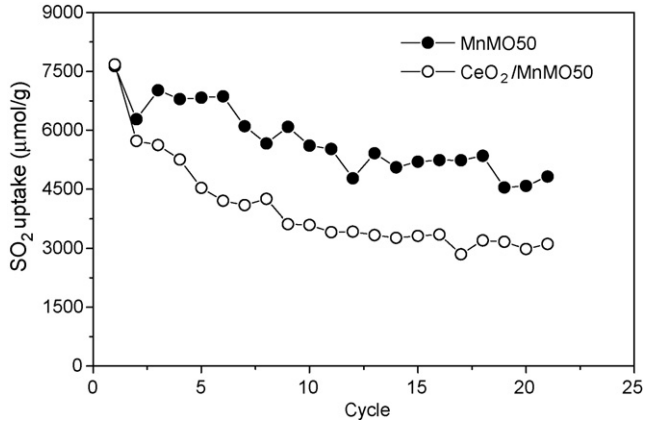


**Fig. 10.** $SO_2$ uptake along the successive cycles of reaction (oxidative adsorption step) and regeneration.

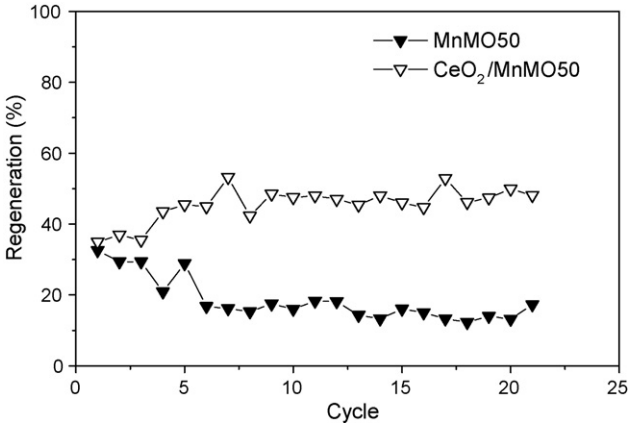


**Fig. 12.** Regeneration (%) of the catalysts along the successive cycles of reaction (oxidative adsorption step) and regeneration.

Fig. 11 compares the release of $H_2S$ and of $SO_2$ in the regeneration step, under the stream of $H_2$/He, at 650 °C, for 5 min, along the 21 cycles. It can be observed that, for both samples, the amount of $H_2S$ released decreased along the cycles and that the formation of $SO_2$ cannot be neglected.

As to the percentage of catalyst regeneration in each cycle (defined as the fraction of sulfur uptaken that was released as $H_2S$ and $SO_2$ in the regeneration step), shown in Fig. 12, it can be observed that after the fifth cycle it remained constant at about 18% and 45% for samples MnMO50 and $CeO_2$/MnMO50, respectively. Taking into account these regeneration levels, it could be expected a nearly complete deactivation of the catalysts, which was not observed. This fact could be associated to the thermal decomposition of the sulfate species that were not reduced in the 5 min regeneration step, during the heating of the additive from 650 to 720 °C, under He, between the cycles. This phenomenon was common to both additives, but the amount of $SO_2$ released was particularly important for the catalyst MnMO50. This could explain why the deactivation was smaller for this catalyst along the successive reaction–regeneration cycles.

For sample $CeO_2$/MnMO50, an unexpected release of $SO_2$ was observed at the beginning of the oxidative adsorption step of cycles 2 to 21 and was associated to a partial oxidation of MnS that remains in the regenerated additive by the oxidant atmosphere of the oxidative adsorption step. This reaction would be promoted by $CeO_2$, since it was not observed for sample MnMO50.

$$MnS(s) + 3/2O_2(g) \rightarrow MnO(s) + SO_2(g) \quad (5)$$

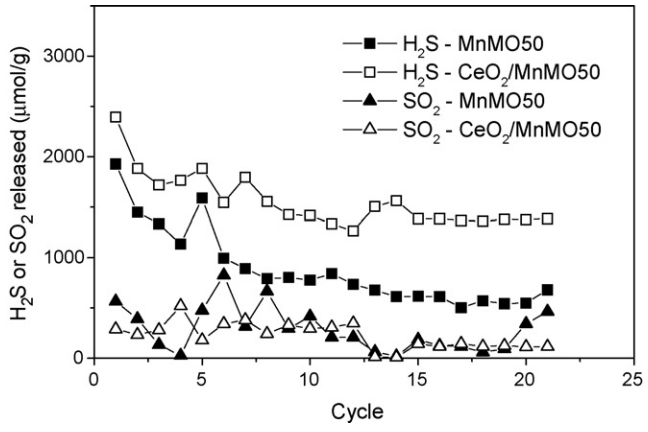


**Fig. 11.** $H_2S$ and $SO_2$ released in the regeneration step along the successive cycles of reaction (oxidative adsorption step) and regeneration.

The presence of MnS can also contribute to the deactivation of Mn-containing catalysts, since this species is not active for promoting neither the oxidation of $SO_2$ nor the fixation of $SO_3$.

It is important to notice that for a real process in the FCC unit, the presence of MnS in the regenerated catalyst is not a problem, since it can be hydrolyzed in the stripper to form the original oxide [4,12].

$$MnS(s) + H_2O(g) \rightarrow MnO(s) + H_2S(g) \quad (6)$$

Concerning the stability of the catalysts after 21 cycles, $CeO_2$/MnMO50 sample presented a lower $SO_2$ uptake efficiency than MnMO50, which was associated to the largest deactivation occurred in the first cycles. However, ceria incorporation had a beneficial effect regarding the reduction of the sulfated species during the regeneration step (30% $H_2$/He, at 650 °C for 5 min). The fraction of $CeO_2$/MnMO50 catalyst regenerated was always higher and the amount of $SO_2$ released in the reduction process was significantly lower than those observed for sample MnMO50. Thus, since the loss of sulfur uptake capacity is related to the pore blockage by sulfate species [9], the smaller deactivation observed for MnMO50 could be justified taking into account the more significant thermal decomposition of the unreduced sulfate species observed for this sample between the cycles, when temperature was raised from 650 to 720 °C under He flow. This fact can be tentatively explained by suggesting that the presence of $CeO_2$ favors the sulfate species reduction but not its thermal decomposition.

## 4. Conclusions

The increase in the $Al/(Al + M^{2+})$ molar ratio from 0.25 to 0.50 improves the performance of Mg,Mn,Al-oxides with spinel structure as catalysts for $SO_x$ abatement. The reduction of the sulfated catalysts was not observed at 530 °C (typical temperature of the *riser of FCC* units). However, with the gradual increase in temperature up to 800 °C (TPR stage), the partial regeneration of samples MnOM25 and MnOM50 was observed. The incorporation of $CeO_2$ to sample MnMO50 increased the amount of $SO_x$ uptake for lower reaction times (10 min) and favored the regeneration of the sulfated catalysts, although did not affect the reduction profiles. Under these experimental conditions, $H_2S$ was the only reduction product.

The increase in TOS for the oxidative adsorption step increased the amount of $SO_x$ uptaken and when the regeneration of these sulfated additives was evaluated at 650 °C (temperature of the base of the riser) the release of $SO_2$ preceded that of $H_2S$.

As to the performance along successive reaction–regeneration cycles, deactivation was observed during this process. $H_2S$ and $SO_2$ (smaller amount) were detected as regeneration products. Although the incorporation of $CeO_2$ has increased the regeneration efficiency and favored a lower formation of $SO_2$ as product of the reduction of the sulfated species, $CeO_2$/MnMO50 presented a lower $SO_x$ uptake efficiency after 21 successive cycles of reaction–regeneration than the sample without ceria (MnMO50). This was associated to the thermal decomposition of the unreduced sulfate species between the cycles that also contributed to the recovery of $SO_x$ uptake capacity but occurred in lower extension on the $CeO_2$-containing sample.

## Acknowledgement

C.A. Henriques would like to thank PROCIENCIA Program of Universidade do Estado do Rio de Janeiro for the financial support.

## References

[1] B. Wen, M. He, C. Costello, Energy Fuels 16 (2002) 1048.
[2] W.-C. Cheng, G. Kim, A.W. Peters, X. Zhao, K. Rajagopalan, Catal. Rev. Sci. Eng. 40 (1998) 39.
[3] A.E. Palomares, J.M. Lópes-Nieto, F.J. Lázaro, A. Lópes, A. Corma, Appl. Catal. B 20 (1999) 257.
[4] A. Corma, A.E. Palomares, F. Rey, Appl. Catal. B 3 (1994) 29.
[5] A. Corma, A.E. Palomares, F. Rey, F. Márques, J. Catal. 170 (1997) 140.
[6] J.A. Wang, L.F. Chen, R. Ballesteros, A. Montoya, J.M. Dominguez, J. Mol. Catal. A: Chem. 194 (2003) 181.
[7] J.S. Yoo, A.A. Bhattacharyya, C.A. Radlowski, J.A. Karch, Appl. Catal. B 1 (1992) 169.
[8] J.A. Wang, C.L. Li, Appl. Surf. Sci. 161 (2000) 406.
[9] C.M.S. Polato, C.A. Henriques, A. Alcover Neto, J.L.F. Monteiro, J. Mol. Catal. A: Chem. 241 (2005) 184.
[10] C.M.S. Polato, J.L. Monteiro, C.A. Henriques, Catal. Today 133–135 (2008) 534.
[11] J.A. Wang, Z.L. Zhu, C.L. Li, J. Mol. Catal. A: Chem. 139 (1999) 31.
[12] A.A. Bhattacharyya, G.M. Woltermann, J.S. Yoo, J.A. Karch, W.E. Cormier, Ind. Eng. Chem. Res. 27 (1988) 1356.
[13] G. Kim, M.V. Juskelis, Stud. Surf. Sci. Catal. 101 (1996) 137.
[14] G. Centi, S. Perathoner, Catal. Today 127 (2007) 219.
[15] G. Centi, S. Perathoner, Appl. Catal. B 70 (2007) 172.
[16] S. Velu, N. Shah, T.M. Jyothi, S. Sivasanker, Microporous Mesoporous Mater. 33 (1999) 61.
[17] K. Jirátová, P. Cuba, F. Kovanda, L. Hilaire, V. Pitchon, Catal. Today 76 (2002) 43.
[18] M. Stoyanova, St. Christoskova, M. Georgieva, Appl. Catal. A 249 (2003) 295.
[19] M. Astier, E. Garbowski, M. Primet, Catal. Lett. 95 (2004) 31.
[20] L. Li, D.L. King, Ind. Eng. Chem. Res. 44 (2005) 168.
[21] K. Tikhomirov, O. Kröcher, M. Elsener, M. Widmer, A. Wokaun, Appl. Catal. B 67 (2006) 160.
[22] C.M.S. Polato, J.L. Monteiro, C.A. Henriques, Quim. Nova 32 (2009) 38.
[23] C.M.S. Polato, A.C.C. Rodrigues, J.L. Monteiro, C.A. Henriques , Ind. Eng. Chem. Res. (submitted).
[24] R.E. Roncolatto, M.J.B. Cardoso, Y.L. Lam, M. Schmal, Ind. Eng. Chem. Res. 45 (2006) 2646.
[25] ICDD PDF-2 Database (Release 1998)–ICDD. 12 Campus Boulevard Newton Square, Pensylvania, USA.
[26] F. Cavani, F. Trifiró, A. Vacari, Catal. Today 11 (1991) 173.
[27] H.B. Pereira, C.M.S. Polato, J.L.F. Monteiro, C.A. Henriques, Proc. 14th Brazilian Congress on Catalysis, Porto de Galinhas, 16–19 September, 2007, CDRom.
[28] A. Trovarelli, C. Leitenburg, M. Moaro, G. Dolcetti, Catal. Today 50 (1999) 353.
[29] H.B. Pereira, C.M.S. Polato, A.C.C. Rodrigues, M.L.L. Paredes, J.L.F. Monteiro, C.A. Henriques, Proc. 14th Brazilian Congress on Catalysis, Porto de Galinhas, 16–19 September, 2007, CDRom.